

Role of Dirac nodal lines and strain on the high spin Hall conductivity of epitaxial IrO₂ thin films

Arnab Bose^{1*}, Jocienne N. Nelson², Xiyue S. Zhang¹, Rakshit Jain², D. G. Schlom^{3,4}, D. C. Ralph^{2,4}, D. A. Muller^{1,4}, K. M. Shen^{2,4} and R. A. Buhrman¹

¹ School of Applied and Engineering Physics, Cornell University, Ithaca, New York 14853, United States

² Department of Physics, Cornell University, Ithaca, New York 14853, USA

³ Department of Materials Science and Engineering, Cornell University, Ithaca, New York 14853, US

⁴ Kavli Institute at Cornell for Nanoscale Science, Ithaca, New York 14853, United States

* ab2729@cornell.edu

Abstract

We report *spin-torque ferromagnetic resonance* (ST-FMR) studies of the efficiency (ξ_{DL}) of the damping-like spin-orbit torque exerted on an adjacent ferromagnet film by current flowing in epitaxial (001) and (110) IrO₂ thin films. Angle resolved photoemission spectroscopy studies have shown IrO₂ exhibits *Dirac nodal lines* (DNL) in the band structure, which could enable a very high spin Hall conductivity, σ_{SH} . The (001) films exhibit exceptionally high ξ_{DL} ranging from 0.45 at 293 K to 0.65 at 30 K which sets the lower bounds of σ_{SH} to be $1.9 \times 10^5 \Omega^{-1} m^{-1}$ and $3.75 \times 10^5 \Omega^{-1} m^{-1}$ respectively, ten times higher and of opposite sign than the theoretical prediction. We observe a substantial reduction of σ_{SH} in anisotropically-strained (110) films, which suggests that the DNLs that are present in the (001) films and contribute to σ_{SH} , are disrupted and gapped due to the large anisotropic strain in (110) films, which in turn significantly lowers ξ_{DL} .

Keywords: *complex oxide heterostructures, spin-orbit torques, intrinsic spin Hall conductivity, Dirac nodal lines (DNL), spin-torque ferromagnetic resonance (ST-FMR)*

Since the discovery of a “giant” spin Hall effect (SHE)¹ in certain heavy metal elements there has been an intense effort to identify and develop new and technologically viable, heavy-metal-based thin film materials that could generate spin currents with even greater efficiency to exert spin-orbit torques (SOT)² on adjacent ferromagnetic nanostructures. In parallel, there have been wide ranging fundamental studies of the spin currents that can arise from robust, intrinsic spin-orbit interaction (SOI) effects in more exotic systems including topological insulators^{3,4}, transition metal dichalcogenides with broken crystalline symmetry⁵, Weyl⁶ and Dirac semimetals⁷ where gapless electronic excitations are protected by topology and symmetry. Here we experimentally study strong SOT from the topological semimetal IrO₂ in (001) and (110) normal films, which exhibit distinctly different SHE strengths. The high resistivity (001) films have a quite high spin Hall conductivity (SHC) with behavior indicative of being

in the “*dirty metal regime*”, while the anisotropically strained (110) films have a substantially smaller SHC and are in the “*clean metal regime*”.

A recent focus of SOT research has been the semimetallic SrIrO₃ where theoretical calculations and ARPES indicate that the tilt of the IrO₆ octahedra in the orthorhombic phase leads to narrow t_{2g} conduction bands with near-degeneracies and band crossings protected by the nonsymmorphic crystal symmetry^{8,9,10}. SOT measurements on SrIrO₃/FM bilayers show a large effective-SHC $\sigma_{SH}^{eff} \sim 10^5 \Omega^{-1} m^{-1}$ ^{11,12,13,14}. Here $\sigma_{SH}^{eff} \equiv T_{int} \sigma_{SH}$, where $T_{int} (< 1)$ is the interfacial spin transparency and σ_{SH} is the actual SHC of the material. It is intriguing that Ref 11 and 12 report *opposite signs* of ξ_{DL} and also, a significant in-plane crystalline anisotropy is reported for ξ_{DL} in Ref. 11,13, but not in Ref. 12. The simplest iridate is IrO₂ which in the rutile phase consists of chains of edge-sharing IrO₆ octahedra running along the c -axis with corner-

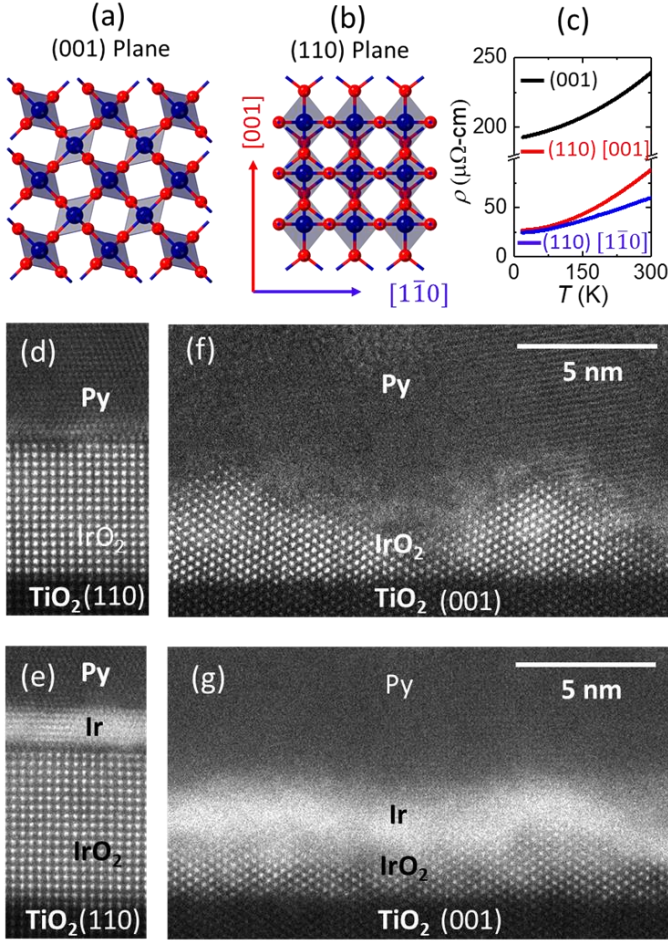


Figure 1. (a), (b) Schematic top-down view representation of the (001) and (110) plane of IrO₂ illustrating the edge to corner connectivity of the octahedra in the (001) plane as opposed to the corner to corner and edge to edge connectivity in the (110) plane. (c) Resistivity of (001) and (110) IrO₂ films as a function of temperature and for the two different principal axes [1 $\bar{1}$ 0] and [001] of the (110) film. (d-g) Annular dark field STEM image of (110) IrO₂/Py, (110) IrO₂/Ir/Py, (001) IrO₂/Py and (001) IrO₂/Ir/Py respectively.

sharing connections among counter-rotated neighboring chains in the (001) plane. Due to the mixture of both edge and corner sharing IrO₆ octahedra, and a relatively direct coordination between Ir atoms that provides an additional hopping channel, the overall result is increased *p-d* orbital hybridization, which broadens the *t*_{2g} conduction band compared to other, corner-sharing, iridates^{9,10}. This reduced electron correlation, which also is found in tetragonal SrIrO₃ where neighboring

octahedra are not counter-rotated and similarly results in larger bandwidths, might suggest that IrO₂ would be a material with a relatively low SHC, as is reported for tetragonal SrIrO₃¹¹. Recent *ab initio* density functional theory (DFT) calculations, however, indicate that the IrO₂ band-structure contains two types of Dirac nodal lines (DNLs) associated with the nonsymmorphic crystal symmetry and the rutile structure¹⁵. Type-1 DNLs allow an anticrossing near the Fermi surface due to SOI and can therefore contribute a large SHC with a maximum value of $-2.5 \times 10^4 (\hbar/2e) \Omega^{-1} \text{m}^{-1}$ ¹⁵, roughly in accord with the results of an early inverse-SHE study of polycrystalline/amorphous IrO₂ films, although of opposite sign¹⁶. Subsequent ARPES studies confirmed the existence of these DNLs in epitaxial IrO₂ thin films and bulk crystals^{17,18}.

Here we report values of $\sigma_{\text{SH}}^{\text{eff}}$ for (001) and (110) IrO₂ films grown epitaxially on TiO₂ rutile substrates as determined by ST-FMR measurements of the efficiency of the damping-like ξ_{DL} and field-like ξ_{FL} spin torques, exerted on an adjacent Ni₈₀Fe₂₀ (Py) thin film. $\sigma_{\text{SH}}^{\text{eff}}$ is then obtained from $\sigma_{\text{SH}}^{\text{eff}} = \xi_{\text{DL}} \sigma_e$, where σ_e is the film's electrical conductivity. Due to the thermodynamically favored reactions between Fe and IrO₂¹⁹ and the unavoidable presence of undercoordinated O ions at the surfaces of a rutile film²⁰, the Fe in the Py near the interface becomes oxidized if deposited directly on the IrO₂. We therefore inserted a thin Ir passivation layer (~1 nm) between the IrO₂ and the Py to avoid this oxidation (Figure 1d-g). (We have determined that Ir has a minimal SHE, $\xi_{\text{DL}} \leq 0.02$.) Even with the significant spin current attenuation arising from this Ir layer, at room temperature (RT) we determined ξ_{DL} to be 0.45 for current flow in the plane of the low σ_e (001) films, rising to 0.65 at 30K, corresponding to $\sigma_{\text{SH}}^{\text{eff}} = 1.9 \times 10^5 (\hbar/2e) \Omega^{-1} \text{m}^{-1}$ at RT, and $3.75 \times 10^5 (\hbar/2e) \Omega^{-1} \text{m}^{-1}$ at 30 K. These lower bounds are more than an order of magnitude higher, and of opposite sign, than the available theoretical prediction for σ_{SH} ¹⁵. For the (110) IrO₂ films, which are anisotropically-strained, the SHC is substantially reduced while σ_e is increased (Figure. 1c), and both quantities are slightly anisotropic. At RT $\sigma_{\text{SH}}^{\text{eff}}$ varies from $7.8 \times 10^4 (\hbar/2e) \Omega^{-1} \text{m}^{-1}$ to $8.8 \times 10^4 (\hbar/2e) \Omega^{-1} \text{m}^{-1}$ between the lower conductivity [001] and higher conductivity [1 $\bar{1}$ 0] directions. The

anisotropy in σ_{SH}^{eff} increases as σ_e increases with decreasing temperature (T), with σ_{SH}^{eff} becoming $9.6 \times 10^4 \Omega^{-1} m^{-1}$ and $1.85 \times 10^5 \Omega^{-1} m^{-1}$, respectively, at 30 K. We attribute the large reduction of σ_{SH}^{eff} in the anisotropically-strained (110) IrO₂ compared to isotropically-strained (100) IrO₂ as being due to disruption of the type-1 DNLs by the anisotropic strain.

For this study, we grew IrO₂ thin films of 5 nm thickness by reactive oxide molecular beam epitaxy (MBE) on (001) and (110) single crystal TiO₂ substrates at room temperature, as described in Supporting Information²¹ and in Ref. 9,10,22,23. The IrO₂ grows centrosymmetrically on (001) TiO₂, with a coherent, isotropic in-plane biaxial tensile strain of $\epsilon_{11} = \epsilon_{22} \approx 2\%$. The nonsymmorphic symmetry is preserved under this isotropic strain. In contrast the (110) films grow with a compressive strain ($\sim -5\%$) in the [001] direction and a tensile strain ($\sim 2\%$) in the $[\bar{1}\bar{1}0]$ direction films due to the lattice mismatch between IrO₂ and (110) TiO₂. It has been found that this anisotropic strain for (110) IrO₂ films persists up to at least a 16 nm thickness¹⁰. This strain breaks the nonsymmorphic symmetry of the (110) films.

The T -dependent resistivities of the different films and for different current directions in the (110) case are shown in Figure 1c. The resistivity of the (001) film, which is independent of the direction of current flow, is high and exhibits only a small residual resistivity ratio (RRR). The (110) films have a lower resistivity and higher RRR, indicative of a cleaner metal, with the resistivity being dependent upon direction of the current flow. This anisotropy does not, however, appear to be due primarily to the anisotropic strain in these films since the nearly 50% difference in resistivity at RT between current flow in the [001] and $[\bar{1}\bar{1}0]$ directions, Figure 1c, is roughly consistent with the 77% difference in resistivity at RT in unstrained IrO₂ single crystals^{24,22}.

For the ST-FMR measurements^{25,26,27} four series of multilayers were prepared as described in Ref 21. Series 1: (001)IrO₂(5nm)/Ir (1nm)/Py(3-6nm)/TaO_x(1.5nm); Series 2: (110)IrO₂(5nm)/Ir(1 nm)/Py(3-6nm)/TaO_x(1.5nm); Series 3: (001)IrO₂ (5nm)/Py(3-7nm)/TaO_x(1.5nm); and Series 4: (110) IrO₂(5nm)/Py(2.7-7nm)/TaO_x(1.5nm). The multilayers with the Ir passivation layer, Series 1 and 2, were the major focus of the SOT study, while Series

3 and 4 were used to quantify the benefit and cost of the use of the Ir spacer.

Cross-sections of examples of each of the four types of IrO₂ multilayer were examined by high resolution scanning transmission electron microscopy (STEM) and EELS. Annular dark field STEM images of the cross-sections are shown in Figure 1d-g. The epitaxial (110) films are atomically flat on the lateral scale of the cross-sectional image while the Py is polycrystalline, both with and without the textured Ir spacer (Figure 1d-e). The (001) IrO₂ films are quite faceted (Figure 1f-g), consistent with the high surface energy of the (001) rutile surface²⁸. The faceted IrO₂ (001) surface is most clearly seen in the sample without the Ir spacer (Figure 1f) as the latter wets the surfaces of the IrO₂ facets, obscuring the dark-field contrast with the Py. Spatially resolved EELS measurements show that the Ir is quite effective in passivating the surface of the IrO₂ for both the (110) and the faceted (001) films, with there being no signal of oxidized Fe atoms²¹. For the samples without the Ir spacer, the EELS data indicate significant Fe oxidation in the vicinity of the IrO₂ surface for the faceted (001) films. There is less Fe oxide at the unpassivated (110) IrO₂ surface, consistent with the lower density of under-coordinated O ions at the (110) rutile surface.

The details of the ST-FMR technique we used are provided in the Ref 21. In brief we measure the FMR resonant response to a microwave current applied to the HM/FM coplanar waveguide in the presence of an in-plane magnetic field. This response consists of a symmetric Lorentzian voltage signal of amplitude S centered about the resonant field H_0 due to the in-plane damping-like torque, and an antisymmetric Lorentzian response, of amplitude A , to the out-of-plane torque resulting from the microwave Oersted field generated by the current flowing in the HM, plus any additional interfacial field-like torque contribution from the incident spin current. The result can be expressed in term of a quantity ξ_{FMR} ²⁶ where

$$\frac{1}{\xi_{FMR}} \equiv \frac{\frac{A(\hbar)}{S(e)}}{\left(\mu_0 M_s d_{Py} d_{IrO_2} \sqrt{1 + \left(\frac{M_{eff}}{H_0}\right)^2}\right)} = \frac{1}{\xi_{DL}} \left(1 + \frac{\hbar}{e} \frac{\xi_{FL}}{\mu_0 M_s d_{Py} d_{IrO_2}} \right) \quad \text{Eqn. 1.}$$

Here d_{Py} and d_{IrO_2} are the thicknesses of the Py and IrO₂ layers, M_s is the saturation magnetization of the Py as measured by vibrating sample magnetometry and M_{eff} is the Py's out-of-plane demagnetization field.

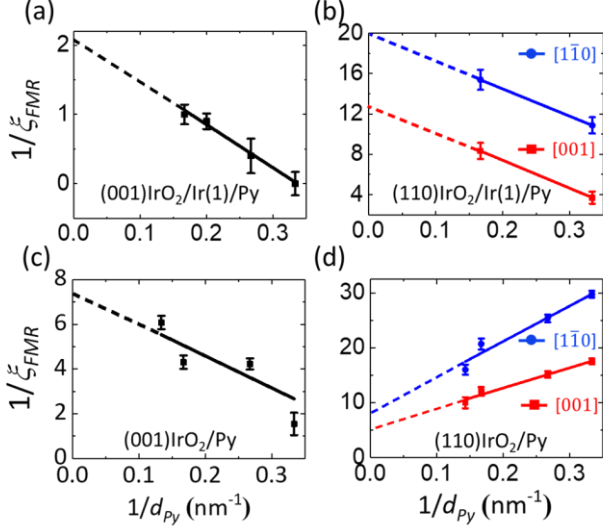


Figure 2. The inverse of the ST-FMR apparent spin torque efficiency ($1/\xi_{\text{FMR}}$) at room temperature as a function of the inverse of Py thickness ($1/d_{\text{Py}}$) for the different series of samples: (a) (001)IrO₂/Ir(1)/Py; (b), (110)IrO₂/Ir(1)/Py for both the $[1\bar{1}0]$ (red color) and $[001]$ directions (black color); (c) (001)IrO₂/Py; and (d) (110)IrO₂/Py.

In **Figure 2**, we show plots of $1/\xi_{\text{FMR}}$ vs. $1/d_{\text{Py}}$ as obtained at RT for all four series of samples. The $1/d_{\text{Py}} = 0$ intercepts of the linear fits to the variation of $1/\xi_{\text{FMR}}$ provide $1/\xi_{\text{DL}}$ while ξ_{FL} is determined from the slope of the linear fit to Eqn. 1. The results are presented in Table I. The high resistivity (001) IrO₂ with the 1 nm passivation layer exhibits an exceptionally high, $\xi_{\text{DL}} = 0.45 \pm 0.03$ (**Figure 2a**), notwithstanding the spin current attenuation of the Ir spacer. The lower resistivity (110) films with the Ir

spacer have lower ξ_{DL} along the $[1\bar{1}0]$ and (001) directions with a smaller anisotropy in $\sigma_{\text{SH}}^{\text{eff}}$ as shown in Table 1.

When the Ir spacer layer was not utilized for the (001) IrO₂ films the result was more than a factor of three degradation of ξ_{DL} from the Ir passivated result (**Figure 2c-d**), which we attribute to the substantial oxidation of the interfacial iron in the Py layer, as revealed by the EELS study²⁶. In contrast, in the absence of the Ir spacer for the (110) samples ξ_{DL} is approximately doubled in amplitude for both the $[1\bar{1}0]$ and $[001]$ directions, and with a sign reversal of ξ_{FL} . We conclude that the degree of interfacial Fe oxidation indicated by EELS for the atomically smooth (110) films is not very detrimental, if at all, to interfacial spin transport. From the (110) results we estimate the Ir spin diffusion length λ_s to be ~ 1.2 nm, consistent with a recent work²⁹. This results in the attenuation of the spin current entering the Ir layer from the IrO₂ by approximately 50% before it impinges on the Py.

We measured the SOTs of the Ir passivated samples from RT to 30 K, with the results shown in **Figure 3**. For the high-resistivity (001) IrO₂ films both ξ_{DL} and ξ_{FL} increased substantially as T was decreased, with ξ_{DL} reaching 0.65 ± 0.07 at 30 K, and with the proportionate increase in ξ_{FL} being even larger (**Figure 3a**). For both the $[1\bar{1}0]$ and $[001]$ directions of the (110) films ξ_{DL} decreased with decreasing T , with the percentage decrease being the larger for the lower resistivity $[1\bar{1}0]$ direction, while the smaller ξ_{FL} increased substantially for the $[1\bar{1}0]$ direction (**Figure 3b**) and was more or less constant for the higher resistivity $[001]$ direction (**Figure 3c**). The quite variable behavior of ξ_{FL} is suggestive that the role of the interface is more complex than, for example, is the case for typical Pt/FM system.

Parameters	(001) /Ir/Py	(001) /Py	(110) [1 $\bar{1}$ 0]/Ir/Py	(110) [1 $\bar{1}$ 0]/Py	(110) [001]/Ir/Py	(110) [001]/Py
ξ_{DL}	0.45 ± 0.03	0.14 ± 0.01	0.05 ± 0.008	0.12 ± 0.01	0.08 ± 0.01	0.18 ± 0.01
ξ_{FL}	-0.05 ± 0.005	-0.01 ± 0.005	-0.02 ± 0.005	0.04 ± 0.005	-0.02 ± 0.005	0.02 ± 0.005
$\sigma_{\text{SHE}}^{\text{eff}}$ ($10^5 \hbar/2e \Omega^{-1} m^{-1}$)	1.9 ± 0.15	0.57 ± 0.05	0.78 ± 0.11	1.95 ± 0.2	0.88 ± 0.12	2.13 ± 0.2

Table 1: Values for the damping-like and field-like spin torque efficiencies, as measured at room temperature by ST-FMR, for 5 nm epitaxial IrO₂ films with and without a 1 nm Ir passivation layer between the IrO₂ and the Py spin current detector layer.

We have used the results presented in Figure 3a-c along with the measured variation of the resistivity (Figure 1c) to obtain the variation of $\sigma_{\text{SH}}^{\text{eff}}$ for the two different Ir-passivated IrO₂ surfaces, and for the two principal directions of the (110) samples, both as a function of T and σ_e . Results are shown in Figure 3d-e. The T -dependent resistivity indicates that IrO₂ has a metallic behavior (Figure 1c) with electron transport through the t_{2g} conduction band. For the intrinsic SHE it is expected that σ_{SH} should be more or less independent of σ_e in the “*clean metal*” regime where carrier lifetime is not a factor in determining the overall spin Berry curvature (SBC) and hence σ_{SH} ³⁰. However as σ_e decreases, that is as the carrier lifetime becomes shorter, σ_{SH} is expected to degrade, at first gradually and then more rapidly as σ_e decreases further³⁰. Previous studies have examined the transition between the dirty to clean metal regimes of the SHE in Pt-based alloys and composites^{31,32} and

in epitaxial SrRuO₃ thin films³³ which are compared with the IrO₂ films by plotting $\sigma_{\text{SH}}^{\text{eff}}$ vs σ_e (Figure 3e). (We point out that these plots are only qualitative comparisons that do not account for the differences in carrier density and band structure between the different materials.)

The nearly constant $\sigma_{\text{SH}}^{\text{eff}}$ with varying σ_e (temperature) for the (110) IrO₂ film with current flow in the low resistivity $[1\bar{1}0]$ direction suggests that in this case the material is in or near the “*clean metal regime*”, but with a lower value of $\sigma_{\text{SH}}^{\text{eff}}$, with the behavior for the $[001]$ direction showing a somewhat greater variation with σ_e and larger amplitude overall (Figure 3e). The (001) film appears to be well within the “*dirty metal regime*” but still reaches a quite high maximum value of $\sigma_{\text{SH}}^{\text{eff}}$, $3.75 \times 10^5 (\hbar/2e)\Omega^{-1}\text{m}^{-1}$ (Figure 3e). The data

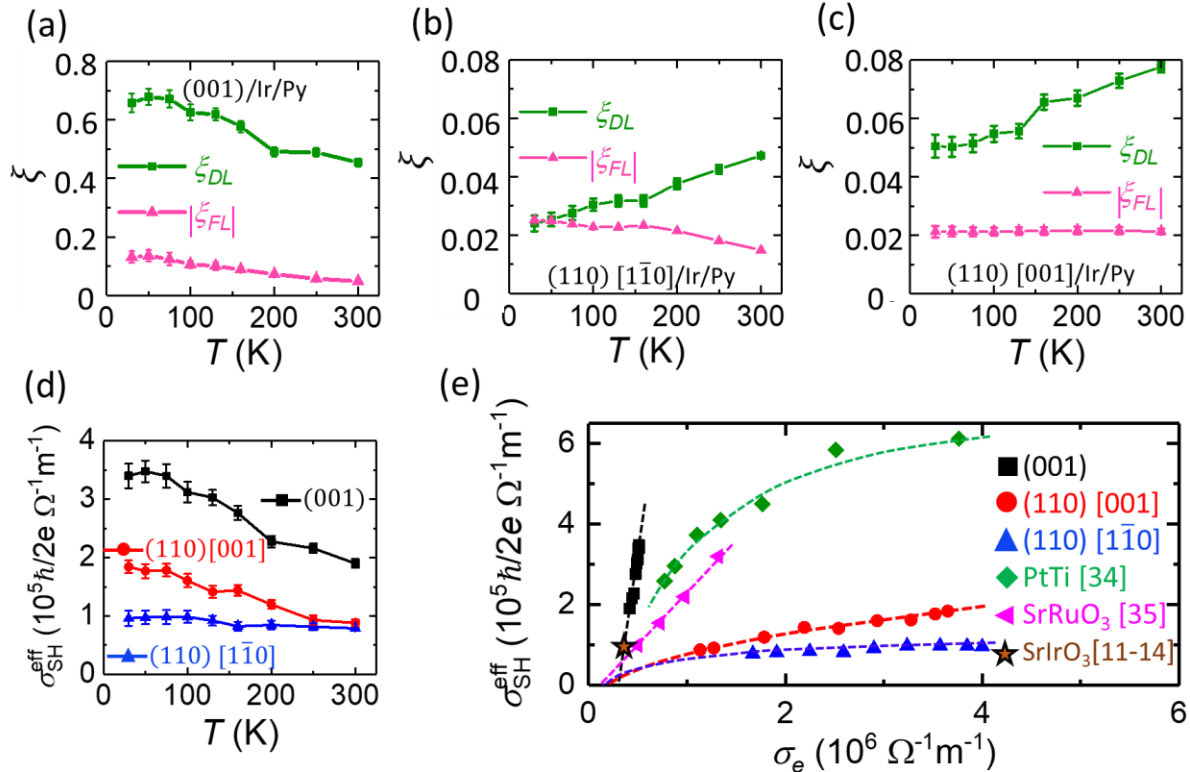


Figure 3. Temperature dependence of ξ_{DL} and $|\xi_{FL}|$ of the Ir passivated samples for the (001) IrO₂/Ir(1)/Py series (a), (110) IrO₂/Ir(1)/Py series in the low resistivity $[1\bar{1}0]$ direction (b) and (110) series along high resistive $[001]$ direction (c). (d) $\sigma_{\text{SH}}^{\text{eff}}$ as a function of temperature for three different cases. (e) $\sigma_{\text{SH}}^{\text{eff}}$ as a function of electrical conductivity (σ_e) of the 5 nm IrO₂ films for the three different cases. Also shown for qualitative comparison are published results of $\sigma_{\text{SH}}^{\text{eff}}$ vs. σ_e for SrRuO₃, SrIrO₃, and 6 nm Pt films where variable numbers of sub-monolayer insertions of Ti were employed to vary σ_e .

suggests that σ_{SH}^{eff} of the (001) film, which is linearly increasing with its σ_e , would further increase and saturate at an even higher value than measured here if a sufficiently higher quality, lower defect density (001) film could be produced with a high enough σ_e to be near or in the clean metal regime. We also note that since the variations in σ_{SH}^{eff} between the different types of epitaxial IrO₂ films and the different current directions of the (110) films do not fall along a common scaling curve as a function of σ_e ($\sigma_{SH}^{eff} = \theta_{SH}\sigma_e$), it appears that the primary cause of the difference is not due to the difference in carrier lifetime.

In seeking a basic understanding of these results we have the challenge that, while the DFT band structure calculations for IrO₂ have generally been experimentally confirmed by ARPES measurements on IrO₂ films, within the accuracy of that technique, although there are discernable differences between measurement and calculation for the anisotropically strained (110) films up to a film thickness of 16 nm,^{10,17} we have measured the SHC to be ~ 10 times the prediction and of opposite sign. (We comment that theoretical underestimation of the SHC is also an issue in simpler spin Hall materials such as Pt and Pt alloys^{31,32}.) While keeping that disagreement in mind we note that the band structure calculations¹⁵ and ARPES measurements show¹⁷, as mentioned above, that the IrO₂ rutile crystal structure possesses two types of DNLs. The DFT calculations predict that the SOC induced anticrossing of bands forming type-1 DNLs near the Fermi energy can provide a large contribution to the SHC. We speculate that the band structure distortion due to the anisotropic strain in the (110) case, and the resulting breaking of the nonsymmorphic crystal symmetry, act to gap the DNLs and suppress the SHC. (A bandgap induced by interactions other than SOC will reduce the SBC.) The distinctly different values and behavior for σ_{SH}^{eff} between the (001) and (110) films, correlated with the absence and presence of anisotropic strain in the two cases, strongly support the role of DNLs, and the effect of strain on them, in determining the amplitude of the SHC, notwithstanding the disagreement between theoretical prediction and experimental results with respect to both amplitude and sign. Along this line of argument, it also seems reasonable to attribute the smaller variation of the

SHC between current flow in $[1\bar{1}0]$ and $[001]$ directions of the (110) plane to the modulation of the SHC by the anisotropic strain in those films. We further note the stark difference between SrIrO₃ and IrO₂ as the (001) IrO₂ film exhibits a three times stronger (six times after correcting spin attenuation though the Ir spacer) SHC than SrIrO₃ which requires octahedral rotation and strong electron correlation to maximize its SHC. It appears that strong electron correlation and a narrow conduction band, by itself, is not essential for obtaining a very high SHC.

In summary, we have measured a very strong, orientation-dependent SHE in epitaxial (001) and anisotropically-strained (110) IrO₂ thin films with σ_{SH} ten times higher and opposite in sign compared to the prediction. Even with the insertion of a 1 nm thick Ir passivation layer, which significantly attenuates the spin current, ξ_{DL} is 0.45 ± 0.03 at RT and 0.65 at 30 K for the higher-resistivity, isotropically strained (001) films. Accounting for the spin attenuation of the 1 nm Ir spacer and assuming T_{int} of approximately 50%, the σ_{sh} would be increased by factor of four. For the (110) films σ_{SH}^{eff} is lower, while still well above the predicted values for IrO₂, and is anisotropic between current flow in the $[1\bar{1}0]$ and $[001]$ directions. We tentatively attribute the lower ξ_{DL} (lower σ_{SH}^{eff}) of the anisotropically strained (110) films, compared to that of the (001) films, to a gapping of the type-1 DNL due to band structure distortion. These results support the theoretical conclusion that the DNLs play a significant role in the large SHE in IrO₂, despite the quantitative disagreement with the magnitude and sign of the experimental results. The (001) film results, combined with the ease of the room temperature growth of IrO₂ epitaxial films, are very promising for application. Achieving a quantitatively correct understanding of the extraordinarily large SHE in a material with strong DNL but a broad t_{2g} conduction band appears to be a continuing theoretical challenge.

Supporting Information

Additional details of the growth and characterization of IrO₂ thin films, sample preparation and ST-FMR measurements and analysis can be found in the Supporting Information.

Author contributions

A.B. and R.A.B. designed the experiment and wrote the first draft the manuscript. A.B. did the sample fabrication, performed the spin torque experiments and analyzed the data. J.N.N. grew the IrO₂ thin films and performed surface characterization with input from K.M.S and D.G.S. STEM images were obtained and analyzed by X.S.Z. with the input from D.A.M. R.J. assisted in the low temperature measurements. D.C.R. provided insightful comments and suggestions through the course of the work. All the authors contributed to discussing the results and the final version of the manuscript. **Competing interests:** The authors declare that they have no competing interests. Data and materials availability: All data needed to evaluate the conclusions in the paper are present in the paper and/or the Supplementary. Additional data is available from authors upon request.

References

- (1) J. Sinova, S. O. Valenzuela, J. Wunderlich, C. H. Back, and T. Jungwirth, Spin Hall effects, *Rev. Mod. Phys.* **2015**, 87, 1213.
- (2) P. M. Haney, H.W. Lee, K. J. Lee, A. Manchon, and M. D. Stiles, Current induced torques, and interfacial spin-orbit coupling: Semiclassical modeling, *Phys. Rev. B.* **2013**, 87, 174411
- (3) A. R. Mellnik, J. S. Lee, A. Richardella, J. L. Grab, P. J. Mintun, M. H. Fischer, A. Vaezi, A. Manchon, E.-A. Kim, N. Samarth, and D. C. Ralph, Spin-transfer torque generated by a topological insulator, *Nature* (London). **2014**, 511, 449.
- (4) Y. Fan et al., Magnetization switching through giant spin-orbit torque in a magnetically doped topological insulator heterostructure, *Nature Mater.* **2014**, 13, 699.
- (5) D. MacNeill, G. M. Stiehl, M. H. D. Guimaraes, R. A. Buhrman, J. Park, and D. C. Ralph, Control of spin-orbit torques through crystal symmetry in WTe₂/ferromagnet bilayers, *Nat. Phys.* **2016**, 13, 300.
- (6) Peng Li, Weikang Wu, Yan Wen, Chenhui Zhang, Junwei Zhang, Senfu Zhang, Zhiming Yu, Shengyuan A. Yang, A. Manchon and Xi-Xiang Zhang, Spin-momentum locking and spin-orbit torques in magnetic nano-heterojunctions composed of Weyl semimetal WTe₂, *Nature Comm.* **2018**, 9, 3990.
- (7) N. P. Armitage, E. J. Mele, Ashvin Vishwanath, Weyl and Dirac semimetals in three-dimensional solids, *Rev. Mod. Phys.* **2018**, 90, 015001.
- (8) Adarsh S. Patri, Kyusung Hwang, Hyun-Woo Lee, and Yong Baek Kim, Theory of Large Intrinsic Spin Hall Effect in Iridate Semimetals, *Scientific Reports.* **2018**, 8, 8052.
- (9) Y.F. Nie, P.D.C. King, C.H. Kim, M. Uchida, H.I. Wei, B.D. Faeth, J.P. Ruf, J.P.C. Ruff, L. Xie, X. Pan, C.J. Fennie, D.G. Schlom, and K.M. Shen, "Interplay of Spin-Orbit Interactions, Dimensionality, and Octahedral Rotations in Semimetallic SrIrO₃, *Phys. Rev. Lett.* **2015**, 114, 016401.
- (10) Jason K. Kawasaki, Masaki Uchida, Hanjong Paik, Darrell G. Schlom and Kyle M. Shen, Evolution of electronic correlations across the rutile, perovskite, and Ruddelsden-Popper iridates with octahedral connectivity, *Phys. Rev. B.* **2016**, 94, 121104(R).
- (11) T. Nan et. al. Anisotropic spin-orbit torque generation in epitaxial SrIrO₃ by symmetry design, *Proc. Nat. Acad. Sci.* **2019**, 116, 16186.
- (12) Hailong Wang, Keng-Yuan Meng, Pengxiang Zhang, Justin T. Hou, Joseph Finley, Jiahao Han, Fengyuan, Yang, and Luqiao Liu, Large spin-orbit torque observed in epitaxial SrIrO₃ thin films, *Appl. Phys. Lett.* **2019**, 114, 232406.

Acknowledgments

We thank Ryan Tapping for providing data on the spin torque efficiency of Ir films. X.S. Zhang thanks Celesta Chang and M. Thomas for assistance with the STEM/EELS studies. Funding: This work was supported in part by the National Science Foundation's MRSEC program (DMR-1719875) through the Cornell Center for Materials Research and the NSF's Platform for the Accelerated Realization, Analysis, and Discovery of Interface Materials (PARADIM) under Cooperative Agreement No. DMR-1539918, by the Office of Naval Research (N00014-19-1-2143), by NSF (DMR-1709255), and by the NSF (ECCS-1542081) through use of the Cornell Nanofabrication Facility/National Nanotechnology Coordinated Infrastructure. R.J. was supported by the US Department of Energy (DE-SC0017671).

- (13) Liang Liu, Qing Qin, Weinan Lin, Changjian Li, Qidong Xie, Shikun He, Xinyu Shu, Chenghang Zhou, Zhishiuh Lim, Jihang Yu, Wenlai Lu, Mengsha Li, Xiaobing Yan, Stephen J. Pennycook and Jingsheng Chen, Current-induced magnetization switching in all-oxide heterostructures, *Nat. Nanotech.* **2019**, 14, 940.
- (14) Arnoud S. Everhardt, Mahendra DC, Xiaoxi Huang, Shehrin Sayed, Tanay A. Gosavi, Yunlong Tang, Chia-Ching Lin, Sasikanth Manipatruni, Ian A. Young, Supriyo Datta, Jian-Ping Wang, and Ramamoorthy Ramesh, Tunable charge to spin conversion in strontium iridate thin films, *Phys. Rev. Mat.* 2019, 3, 051201(R)
- (15) Yan Sun, Yang Zhang, Chao-Xing Liu, ClaudiaFelser and Binghai Yan. Dirac nodal lines and induced spin Hall effect in metallic rutile oxides, *Phys. Rev. B.* 2017, 95, 235104.
- (16) K. Fujiwara, Y. Fukuma, J. Matsuno, H. Idzuchi, Y. Niimi, Y. Otani, and H. Takagi, 5d iridium oxide as a material for spin-current detection, *Nat. Commun.* **2013**, 4, 2893.
- (17) J. N. Nelson, J. P. Ruf, Y. Lee, C. Zeledon, J. K. Kawasaki, S. Moser, C. Jozwiak, E. Rotenberg, A. Bostwick, D. G. Schlom, K. M. Shen, and L. Moreschini. Dirac nodal lines protected against spin-orbit interaction in IrO₂, *Phys. Rev. Mater.* **2019**, 3, 064205.
- (18) X. Xu, J. Jiang, W. J. Shi, Vicky Süß, C. Shekhar, S. C. Sun, Y. J. Chen, S.-K. Mo, C. Felser, B. H. Yan, H. F. Yang, Z. K. Liu, Y. Sun, L. X. Yang and Y. L. Chen, Strong spin-orbit coupling and Dirac nodal lines in the three-dimensional electronic structure of metallic rutile IrO₂, *Phys. Rev. B.* **2019**, 99, 195106.
- (19) I. Barin, *Thermochemical Data of Pure Substances*, **1995**, 3rd Ed., Vol. I and Vol. II (VCH, Weinheim).
- (20) U. Diebold, The surface science of titanium dioxide, *Surface Science Reports* **2003**, 48, 53.
- (21) See Supplemental Material at xxxx for more details on sample fabrication and characterization, and the ST-FMR technique and results.
- (22) Jason K. Kawasaki, Choong H. Kim, Jocienne N. Nelson, Sophie Crisp, Christian J. Zollner, Eric Biegenwald, John T. Heron, Craig J. Fennie, Darrell G. Schlom and Kyle M. Shen, Engineering Carrier Effective Masses in Ultrathin Quantum Wells of IrO₂, *Phys. Rev. Lett.* **2018**, 121, 176802
- (23) Jason K. Kawasaki, David Baek, Hanjong Paik, Hari P. Nair, Lena F. Kourkoutis, Darrell G. Schlom and Kyle M. Shen “Rutile IrO₂/TiO₂ superlattices: A hyperconnected analog to the Ruddelsden-Popper structure, *Phys. Rev. Mater.* **2018**, 2, 054206.
- (24) W. D. Ryden, A. W. Lawson, and C. C. Sartain, Electrical Transport Properties of IrO₂ and RuO₂, *Phys. Rev. B.* **1970**, 1, 1494–1500.
- (25) L. Q. Liu, T. Moriyama, D. C. Ralph, and R. A. Buhrman, Spin-Torque Ferromagnetic Resonance Induced by the Spin Hall Effect, *Phys. Rev. Lett.* **2011**, 106, 036601.
- (26) Chi-Feng Pai, Yongxi Ou, Luis Henrique Vilela-Leao, D. C. Ralph and R. A. Buhrman, Dependence of the efficiency of spin Hall torque on the transparency of Pt/ferromagnetic layer interfaces, *Phys. Rev. B* **92**, **2015**, 064426.
- (27) A. Bose, S. Dutta, S. Bhuktare, H. Singh, and A. A. Tulapurkar, Sensitive measurement of spin-orbit torque driven ferromagnetic resonance detected by planar Hall geometry, *Appl. Phys. Lett.* **2017**, 111, 162405.
- (28) M. Ramamoorthy, D. Vanderbilt, R. D. King-Smith, First-principles calculations of the energetics of stoichiometric TiO₂ surfaces, *Phys. Rev. B.* **1995** 49, 16721.
- (29) Yuto Ishikuro, Masashi Kawaguchi, Naoaki Kato, Yong-Chang Lau and Masamitsu Hayashi, Dzyaloshinskii-Moriya interaction and spin-orbit torque at the Ir/Co interface, *Phys. Rev. B.* **2019**, 99, 134421 (2019).
- (30) T. Tanaka, H. Kontani, M. Naito, D. S. Hirashima, K. Yamada and J. Inoue. Intrinsic spin Hall effect and orbital Hall effect in 4d and 5d metals, *Phys. Rev. B.* **2008**, 77, 165117.
- (31) L. Zhu, L. Zhu, M. Sui, D. C. Ralph, R. A. Buhrman, Variation of the giant intrinsic spin Hall conductivity of Pt with carrier lifetime, *Sci. Adv.* **2019**, 5, eaav8025.
- (32) Lijun Zhu and R.A. Buhrman, Maximizing Spin-Orbit-Torque Efficiency of Pt/Ti Multilayers: Trade Off Between Intrinsic Spin Hall Conductivity and Carrier Lifetime, *Phys. Rev. Applied.* **2019**, 12, 051002.
- (33) Y. Ou, Z. Wang, C. S. Chang, H. P. Nair, H. Paik, N. Reynolds, D. C. Ralph, D. A. Muller, D. G. Schlom and R. A. Buhrman, Exceptionally High, Strongly Temperature Dependent, Spin Hall Conductivity of SrRuO₃, *Nano Lett.* **2019**, 19, 6, 3663...